

Supporting Information:

# **Structural Dynamics of Strongly Segregated Block Copolymer Electrolytes**

Onyekachi Oparaji<sup>a,b</sup>, Suresh Narayanan<sup>c</sup>, Alec Sandy<sup>c</sup>, Subramanian Ramakrishnan<sup>a,b</sup>, and Daniel Hallinan Jr.<sup>a,b,\*</sup>

<sup>a</sup>*FAMU-FSU College of Engineering, Florida A&M University-Florida State University, Tallahassee, Florida 32310, USA*

<sup>b</sup>*The National High Magnetic Field Laboratory, Florida State University, Tallahassee, Florida 32303, USA*

<sup>c</sup>*Argonne National Laboratory, Argonne, Illinois 60439, United States*

\*Corresponding author, [dhallinan@fsu.edu](mailto:dhallinan@fsu.edu), 850-645-0131

**Table S1.** Results of linear regressions to  $d$  versus  $r$  data.

T (°C)	Slope (nm mol <sub>EO</sub> /mol <sub>Li+</sub> )	Intercept (nm)	R <sup>2</sup>
100	282.10	159.00	0.999
120	305.81	159.38	0.991
140	249.46	159.39	0.997
160	247.89	165.12	0.988
180	222.36	170.51	0.994

**Table S2.** Vogel–Fulcher-Tammann (VFT) parameters from temperature dependence of SEO-LiTFSI entanglement relaxation data (rheological experiments).

$r = \frac{[Li^+]}{[EO]}$	0.000	0.020	0.050	0.085	0.105	0.125	0.170
$Rb$ (kJ/mol)	5.47	8.15	8.04	6.05	6.95	16.6	4.39
$\tau_o$ (s)	$3.93 \times 10^{-5}$	$6.51 \times 10^{-7}$	$2.93 \times 10^{-7}$	$3.23 \times 10^{-6}$	$9.14 \times 10^{-5}$	$6.40 \times 10^{-9}$	$4.21 \times 10^{-5}$
$T_o$ (K)	339	332	330	341	314	295	346

**Table S3.** Arrhenius parameters from temperature dependence of SEO-LiTFSI structural relaxation data (XPCS experiments).

$r = \frac{[Li^+]}{[EO]}$	0.000	0.050	0.085	0.125
$E_a$ (kJ/mol)	55.9	66.0	42.4	46.7
$\tau_o$ (s)	$1.03 \times 10^{-5}$	$2.92 \times 10^{-7}$	$5.48 \times 10^{-4}$	$1.46 \times 10^{-4}$

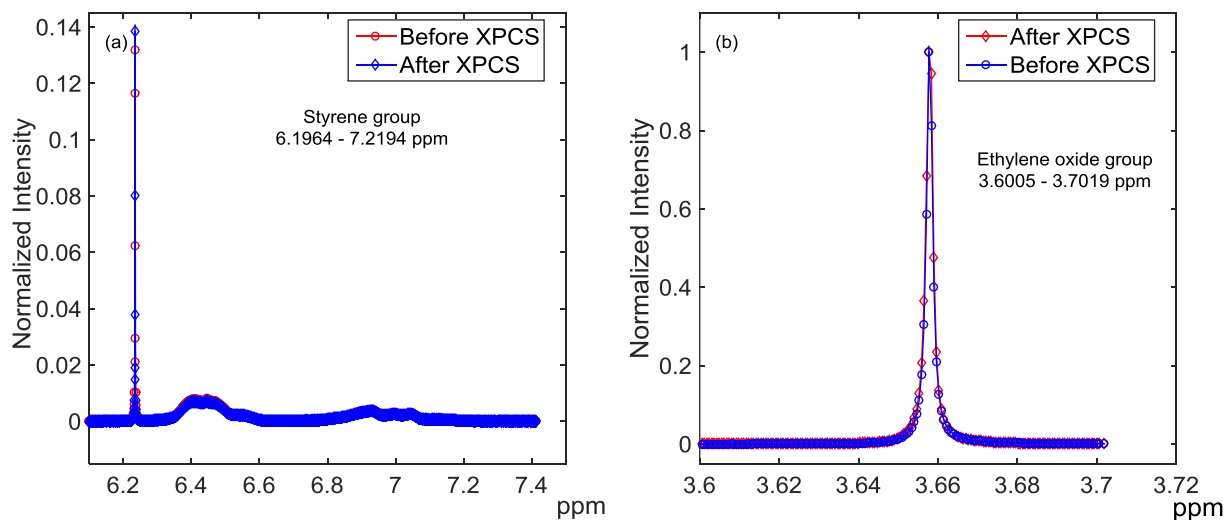


**Figure S1.**  $^1\text{H}$  NMR spectra of SEO block copolymer dissolved in  $\text{CDCl}_3$ , showing proton signals from (a) styrene and (b) ethylene oxide groups before and after XPCS experiments.

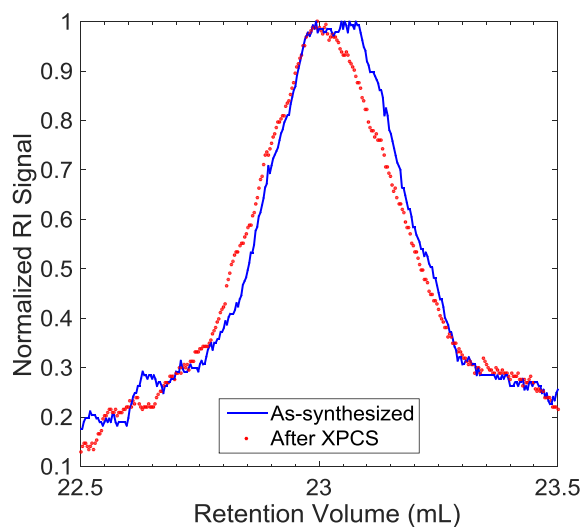


**Figure S2.** GPC traces of the as-synthesized polymer and the polymer ( $r = 0.02 \text{ mol}_{\text{Li}^+}/\text{mol}_{\text{EO}}$ ) after exposure to x-rays during XPCS experiments. Within the resolution of the instrument, there is no difference.

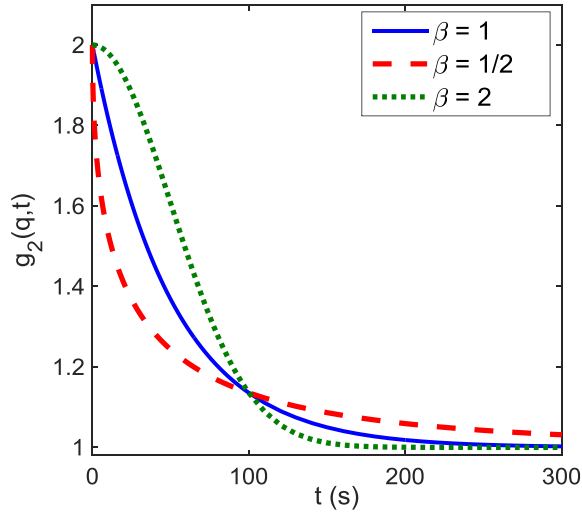


**Figure S3.** Parametric depiction of the KWW function showing exponential decay ( $\beta = 1$ ), stretched exponential decay ( $\beta = 1/2$ ), and compressed exponential decay ( $\beta = 2$ ). At the relaxation time,  $\tau = 100$  s,  $g_2 = 1 + Ae^{-2}$  for all functions;  $A = 1$ .

The stretched exponential ( $\beta < 1$ ) initially decays faster than the simple exponential decay, but then decays more slowly at times greater than  $\tau(q)$ . One can empirically show that such a decay can be approximately reproduced by a superposition of multiple relaxation times. On the other hand, the compressed exponential ( $\beta > 1$ ) is initially slower than the single exponential decay but decays more rapidly near  $\tau(q)$ , approaching the asymptotic limit sooner. The compressed exponential cannot be reproduced by multiple exponential relaxations.

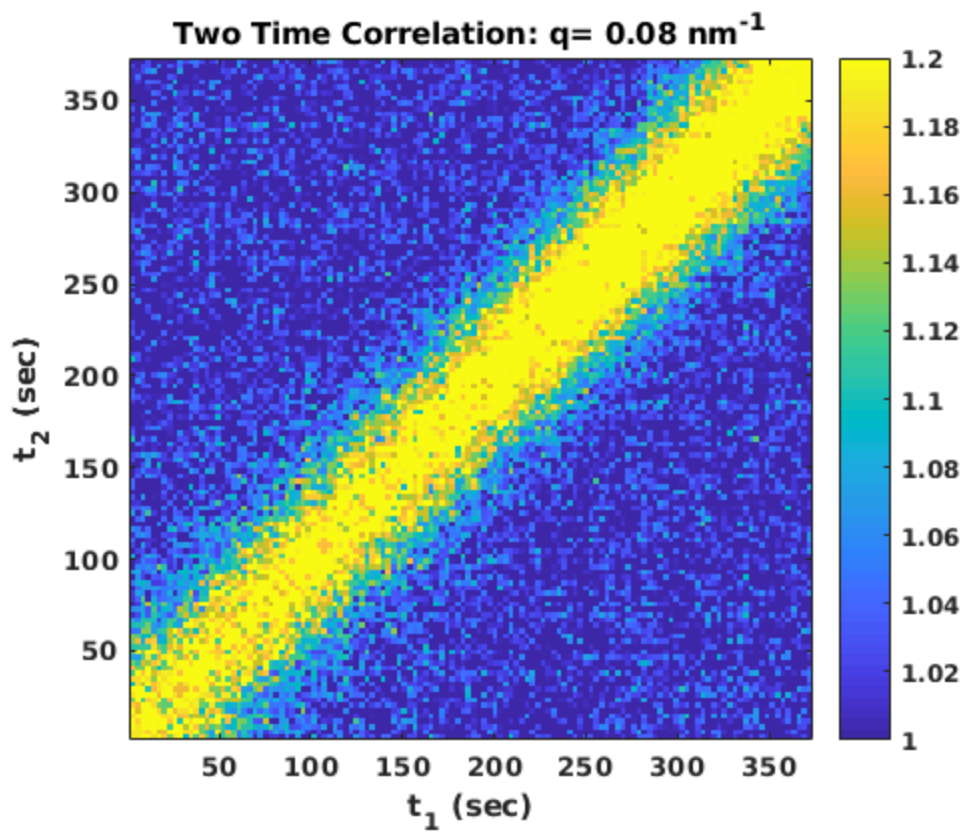


**Figure S4.** Two time correlation of SEO-LiTFSI with  $r = 0.02$  at  $140 \text{ }^\circ\text{C}$  at  $2q^*$ .

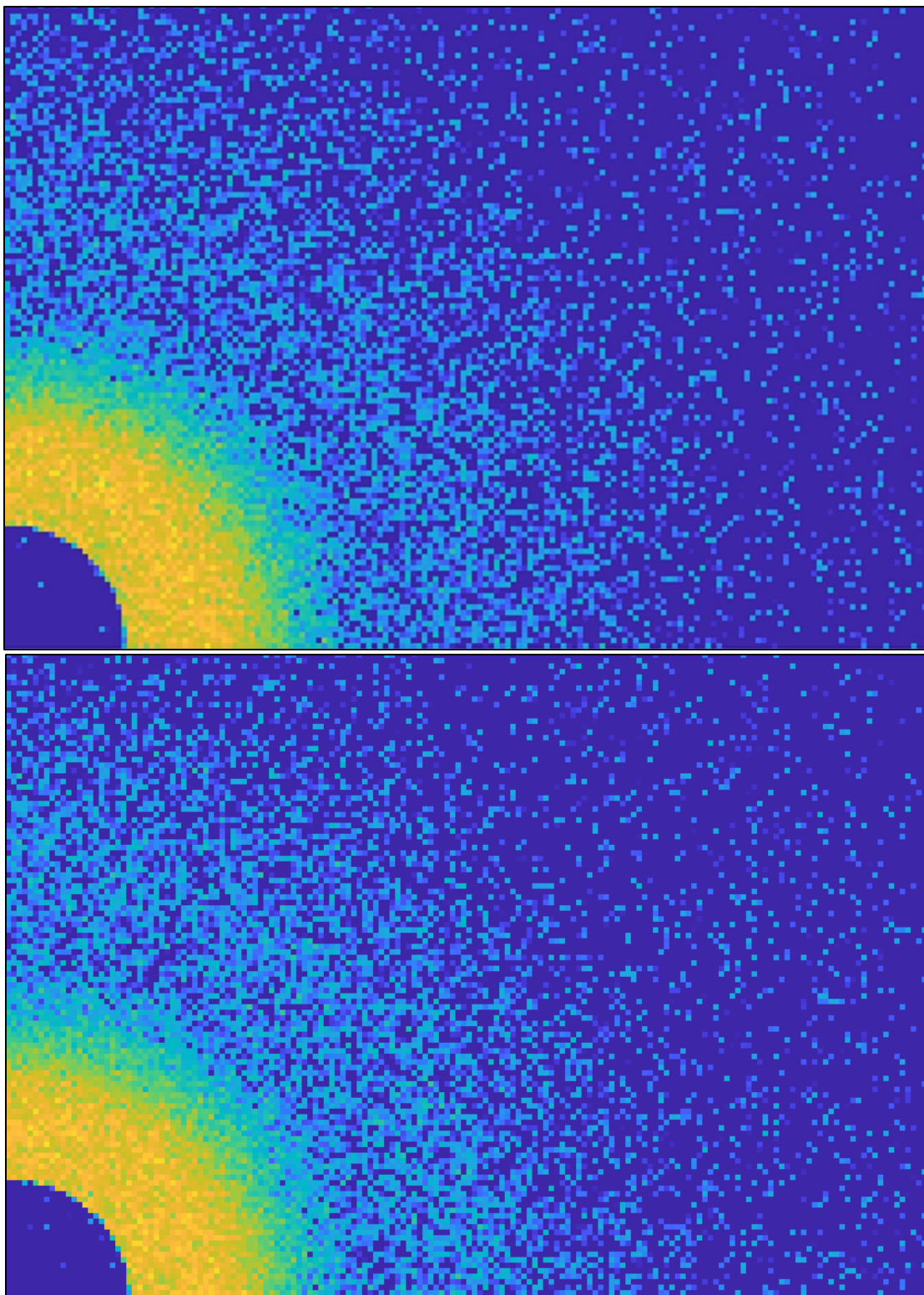


**Figure S5.** Two-dimensional x-ray scattering patterns of salt-free SEO membrane at 140 °C from (Top) the beginning of data collection and (Bottom) the end of data collection. In order to improve signal-to-noise ratio, each 2D pattern is the average of 10 images (e.g. the first 10 or last 10 images of data collection for x-ray photon correlation spectroscopy).

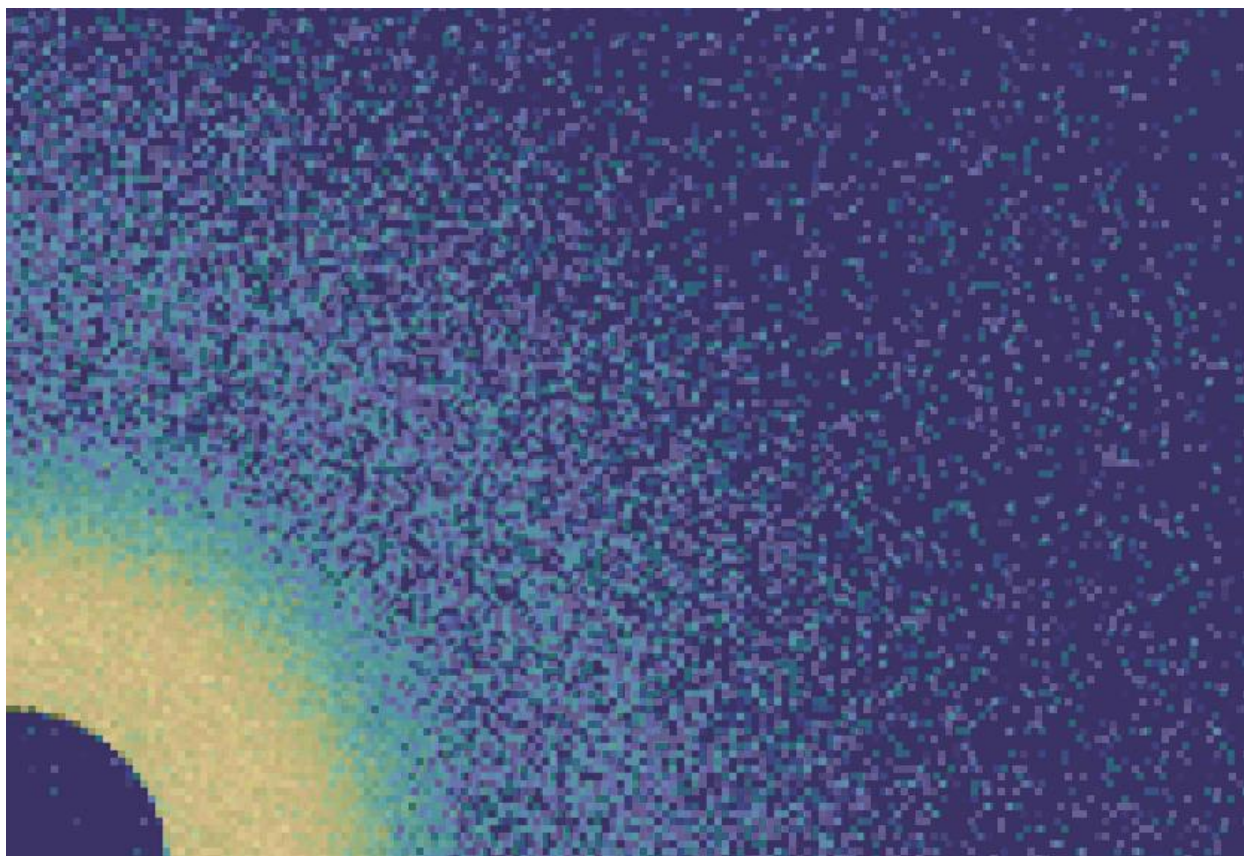


**Figure S6.** Overlay of both 2D images of Figure S5, with bottom image converted to black and white. Top image speckles appear blue throughout most of image, while bottom image speckles appear mauve.

The variation of the Scherrer grain size,  $L$ , of the SEO-LiTFSI as a function of concentration and temperature was determined using  $L = \frac{2\pi}{FWHM}$ . Where FWHM was determined using the expression;  $FWHM = 2 * \sqrt{2 \log 2} * stdev$ ; from a Gaussian fit to the primary scattering peak. Detailed values of FWHM for all conditions are shown in Figure S7a. The grain sizes decrease with increasing temperature and increase with increasing salt concentration.

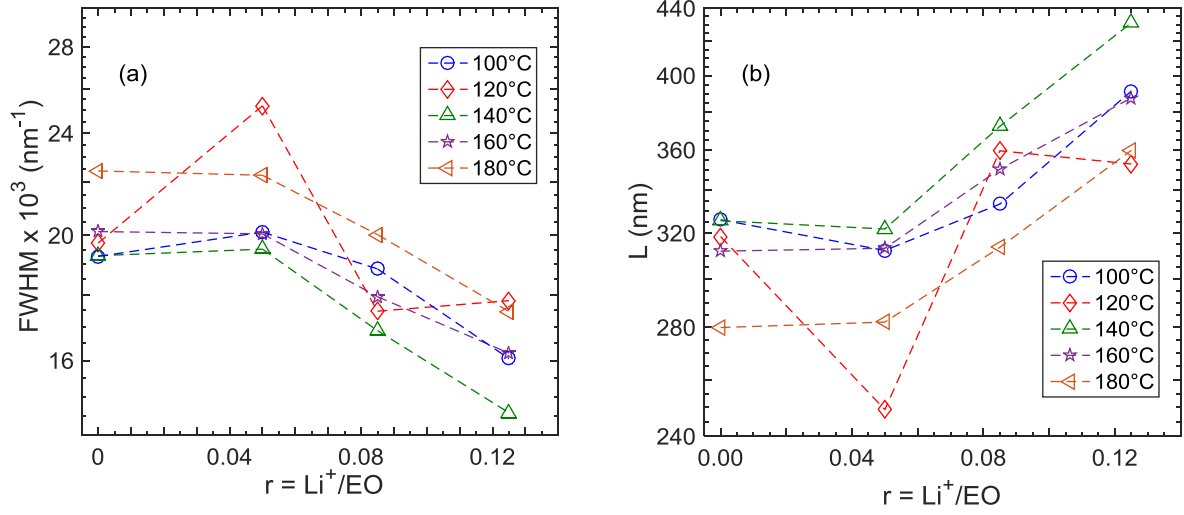


**Figure S7.** (a) Full width at half maximum (FWHM) and (b) grain size ( $L$ ) of SEO-LiTFSI as a function of salt concentration at different temperatures.

Volume additivity was used to predict the increase in domain size with the addition of salt to SEO. Using a basis of 1 mole SEO, the volume ratio of LiTFSI to SEO was calculated as follows:

$$\frac{V_{\text{LiTFSI}}(T)}{V_{\text{SEO}}} = \frac{r x_{\text{PEO}} M_{\text{LiTFSI}} \hat{V}_{\text{LiTFSI}}}{(x_{\text{PEO}} M_{\text{EO}} \hat{V}_{\text{PEO}}(T) + x_{\text{PS}} M_{\text{S}} \hat{V}_{\text{PS}}(T))},$$

The constants are reported in Table S1 and ( $T$ ) denotes that the term is a function of temperature. We did not account for the thermal expansion of the salt. Then the domain spacing,  $d(r, T)$ , at a salt concentration,  $r$ , was calculated as follows:

$$d(r, T) = d(0, T) * \left( 1 + \frac{V_{\text{LiTFSI}}(T)}{V_{\text{SEO}}} \right).$$

The specific volume,  $\hat{V}_i$ , of each phase of SEO ( $i = \text{PEO}$  or  $\text{PS}$ ) was calculated using the thermal expansion coefficients reported in Table S1 (quadratic for PEO and linear for PS) as follows:

$$\hat{V}_i(T) = \alpha_i (T - T_{\text{ref}}) + \beta_i (T - T_{\text{ref}})^2 + \hat{V}_i(T_{\text{ref}}).$$

The domain spacing was then calculated at a given temperature from a reference temperature ( $T_{\text{ref}} = 180 \text{ }^\circ\text{C}$ ) as follows:

$$d(r, T) = d(r, T_{ref}) \left[ \phi_{PEO} \left( 1 + \frac{\hat{V}_{PEO}(T) - \hat{V}_{PEO}(T_{ref})}{\hat{V}_{PEO}(T_{ref})} \right) + \phi_{PS} \left( 1 + \frac{\hat{V}_{PS}(T) - \hat{V}_{PS}(T_{ref})}{\hat{V}_{PS}(T_{ref})} \right) \right]$$

where the volume fractions are  $\phi_i(T) = \frac{x_i M_i \hat{V}_i(T)}{\sum_i x_i M_i \hat{V}_i(T)}$ . The results are shown in Figure S8.

**Table S4.** Physical constants of SEO-LiTFSI components used to calculate volume additivity and thermal expansion of domain spacing. Thermal expansion coefficients for PEO are from a quadratic fit to Zoller and Walsh data for 500 kg/mol PEO between 70.3 °C and 198.7 °C. That for PS is a linear fit to Zoller and Walsh data for 110 kg/mol PS between 100.3 °C and 251.3 °C.<sup>1</sup> The coefficients of determination for both regressions are perfect to 4 significant figures.

	PEO	PS	LiTFSI
$x_i$ (mol <sub>i</sub> /mol <sub>SEO</sub> )	0.33	0.67	
$M_{\text{monomer}}$ (g mol <sup>-1</sup> )	44	104	287
$\alpha_i$ (cm <sup>3</sup> g <sup>-1</sup> K <sup>-1</sup> )	6.17 x 10 <sup>-4</sup>	5.90 x 10 <sup>-4</sup>	
$\beta_i$ (cm <sup>3</sup> g <sup>-1</sup> K <sup>-2</sup> )	7.77 x 10 <sup>-7</sup>		
$T_{\text{ref}}$ (°C)	70.3	100.3	20
$\hat{V}(T_{\text{ref}})$ (cm <sup>3</sup> g <sup>-1</sup> )	0.9148	0.9788	0.7519

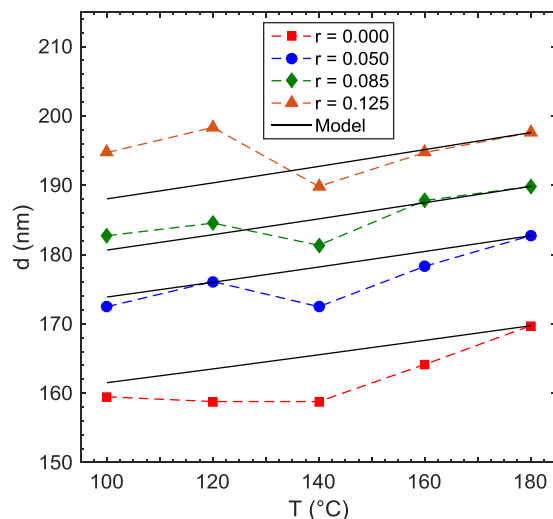


**Figure S8.** Temperature dependence of domain spacing. Lines are volume expansion prediction with  $d(180\text{ °C})$  as reference.

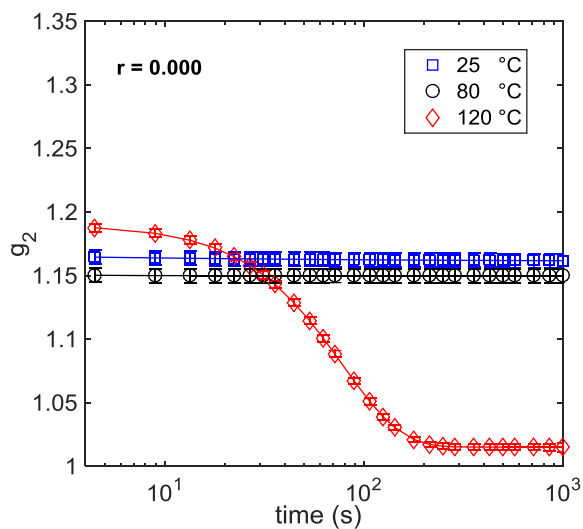


**Figure S9.** Autocorrelation functions obtained from XPCS of SEO without salt ( $r = 0.000$  mol<sub>Li</sub>/mol<sub>EO</sub>) at different temperatures. At 80 and 25 °C (below the  $T_g$  of PS) the lack of decay indicates that there is no motion on the time scale of 5 to 1,000 s. Solid lines denote KWW fits.

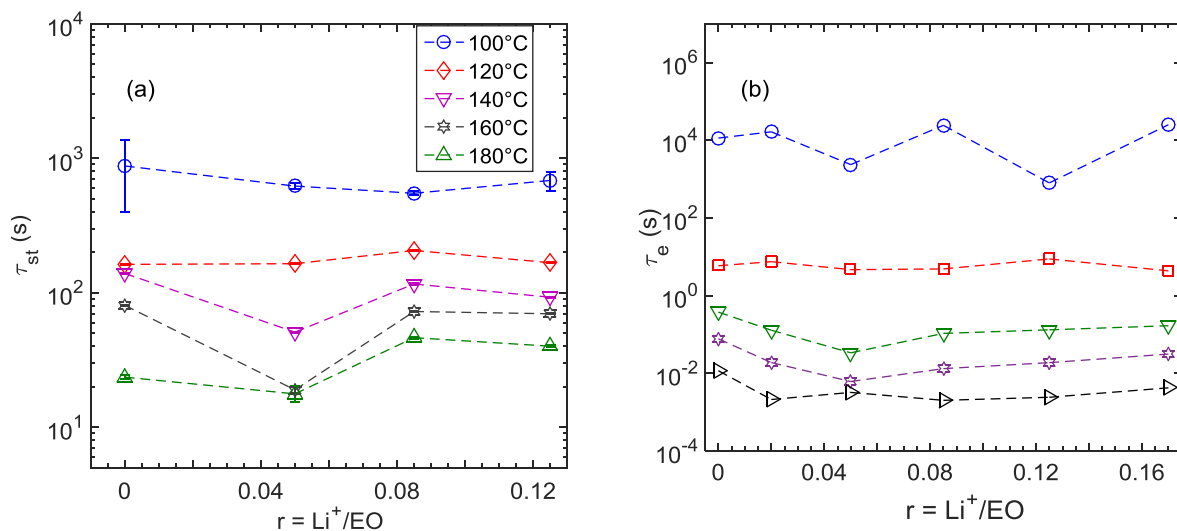


**Figure S10.** (a) Structural relaxation within primary scattering peak region,  $q^*$ . (b) Entanglement relaxation time from rheological measurement. Legend is same as in (a).

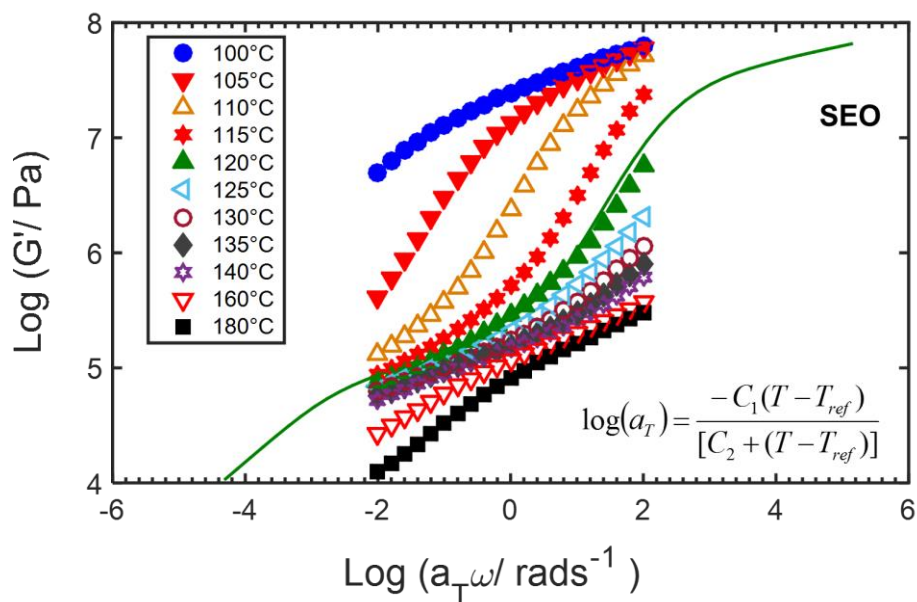


**Figure S11.** Time-temperature superposition of  $G'$  of SEO ( $r = 0.00$ ) with  $T_{ref} = 120$  °C.

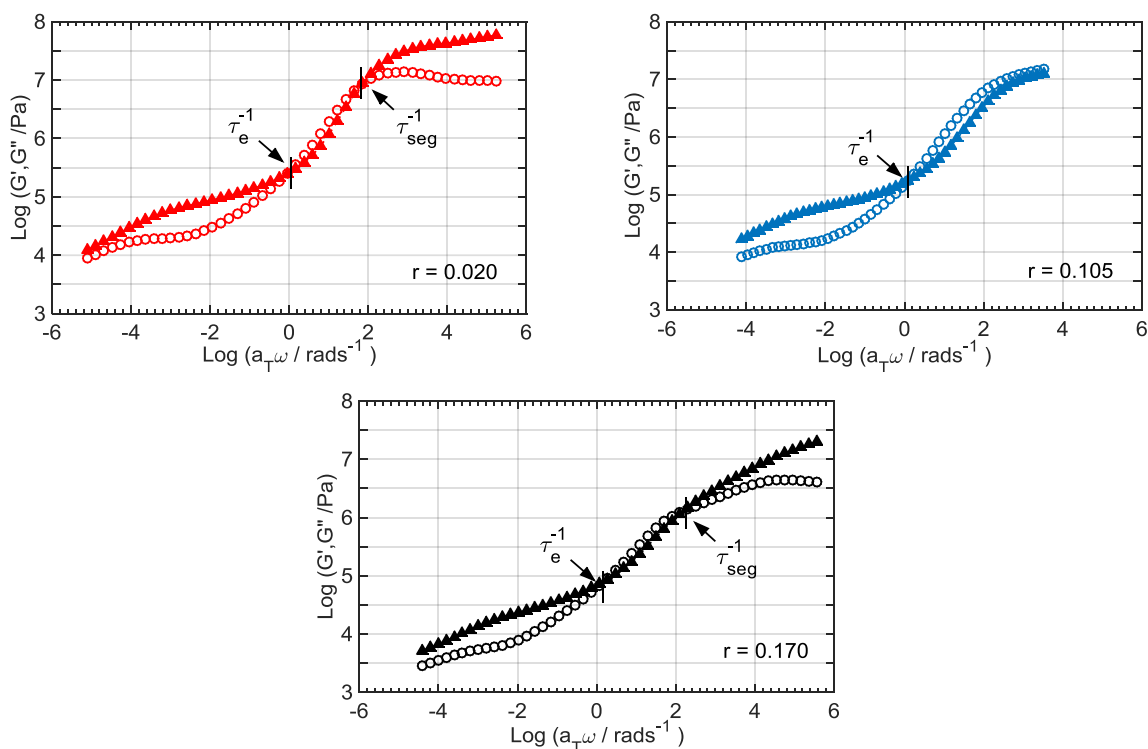


**Figure S12.** Storage and loss moduli of SEO-LiTFSI at different salt concentrations as a function of time-temperature-shifted frequency,  $a_T \omega$ , using a reference temperature of 120 °C.

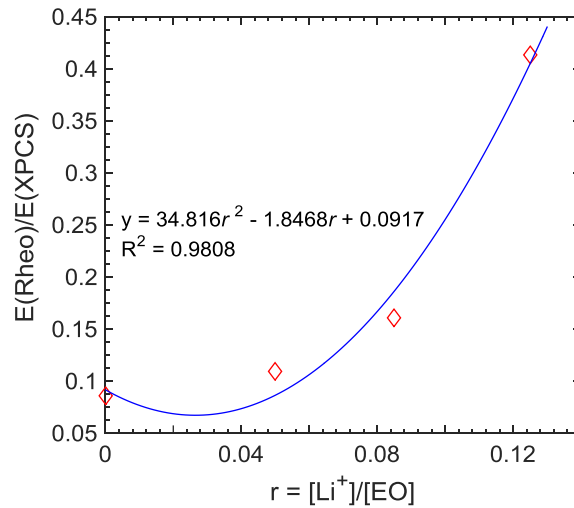


**Figure S13.** Relationship between  $Rb/E_a$  as a function of salt concentration.

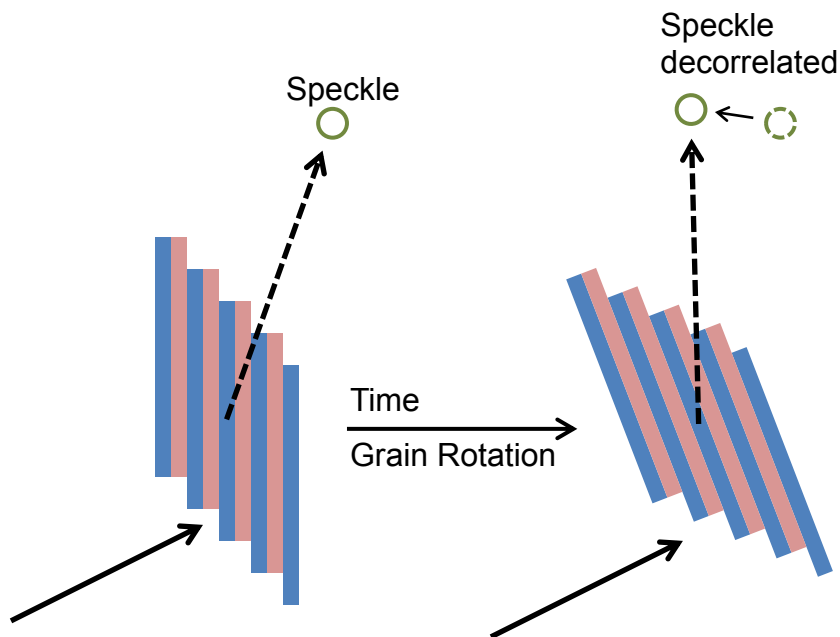


**Figure S14.** Schematic depicting grain rotation, the proposed physical mechanism for structural relaxation in these strongly phase-segregated BCPs.

### Supporting Information References

1. Zoller, P.; Walsh, D. J., *Standard pressure-volume-temperature data for polymers*. Technomic Pub. Co.: Lancaster, PA, 1995; p 412.
2. Langela, M. Struktur und rheologische Eigenschaften von PS-PI und PS-PB Blockcopolymeren. PhD Thesis 2001, Johannes-Gutenberg-Universität Mainz, 2002.